

CALCULATION OF THE MAST PEDESTAL IONISATION PROFILE FROM BOUNDARY PLASMA RECONSTRUCTION

S. Lisgo^{1,2}, G.F. Counsell¹, P. Boerner³, J. Dowling¹, A. Kirk¹, G. Maddison¹,
M. Price¹, D. Reiter³, R. Scannell⁴ and the MAST Team

¹EURATOM/UKAEA Fusion Association, Culham Science Centre, Abingdon, UK

²University of Toronto Institute for Aerospace Studies, Toronto, Canada

³IPP Forschungszentrum Juelich, Juelich, Germany

⁴University College, Cork, Republic of Ireland

Abstract

The accurate prediction of ITER fusion performance requires a reliable scaling of the H-mode pedestal density from present-day tokamaks. It is important therefore to develop a detailed characterization of pedestal ionisation and assess its impact on pedestal parameters, such as density profile height and width. The OSM-Eirene code package, which takes advantage of wide-ranging efforts to improve diagnostic coverage outside the core, is applied to a MAST ELM-free H-mode discharge in an effort to calculate a 2D absolute measure of ionisation in the pedestal region. The simulation agrees with the available D_α constraints within experimental uncertainties ($\sim 30\%$) and indicates that the volume averaged radial ionisation profile is a factor of ~ 2 lower than a 1D estimate based solely on outer midplane measurements.

Introduction

It is predicted that the boundary plasma in next-step tokamaks such as ITER will be opaque to thermal neutrals [1], dramatically reducing pedestal ionization as compared to present-day devices, where neutrals from surface recycling and gas puffing readily penetrate to the confined plasma. It is presently unknown how the absence of this local ionization will affect the density profile, calling into question the validity of empirical pedestal scalings from existing devices. To address this critical issue, there have been numerous efforts to calculate pedestal ionisation and assess the comparative roles played by volume particle sources and plasma transport in the formation of the density pedestal [2–5].

Boundary “plasma reconstruction” is employed in the present study, where experimental data are used to constrain the OSM interpretive plasma code [6], with the solution then input to the Eirene kinetic neutral transport code [7] for calculation of the edge ionization profile. The principal advantages of this semi-empirical approach are the explicit

use of a large number of boundary plasma measurements and flexibility when discretizing the magnetic and structural geometry due to the use of a 1D numerical scheme (plasma transport across field lines is included implicitly via the experimental constraints, allowing the full 2D boundary plasma solution to be developed). Results are presented for an ELM-free H-mode discharge from the Mega-Ampere Spherical Tokamak (MAST) [8].

Experimental setup

MAST is a low aspect ratio ($A = 1.4$) tokamak with a maximum plasma current of 1.5 mega-Amperes and (presently) up to 4 MW of neutral beam power. Resistive heating of the central solenoid limits purely inductive current drive to < 1 s. MAST usually operates in a near double-null (DN) configuration, which will be essential for long-pulse spherical tokamak operation due to the small area available for power deposition on the inboard side [9]. Boronization and inter-shot helium glow discharge cleaning are used for surface conditioning. A unique feature of MAST is the open vessel design, where the poloidal shaping coils are suspended inside the vacuum chamber; see Figure 1. The remote wall creates a large vessel to plasma volume ratio of $\sim 8:1$, which along with the open and extended divertor geometry generates correspondingly large neutral densities in the main chamber on the order of $1-5 \times 10^{18} \text{ D}_2 \text{ m}^{-3}$. This suggests that main chamber fueling of the core dominates, rather than divertor fueling local to the x-points; certainly more so than for most conventional devices where closed divertors and/or close walls are typically employed.

The ELM-free H-mode discharge parameters are $I_p = 0.73 \text{ MA}$, $\bar{n}_e = 3.5 \times 10^{19} \text{ m}^{-3}$, $f_{GW} = 0.5$, $T_0 = 1.1 \text{ keV}$, $B_0 = 0.42 \text{ T}$, $\beta_N = 2.8$ and $P_{NB} = 1.8 \text{ MW}$. Time traces are presented in Figure 2, with the analysis focusing on the plasma state at 259 ms (vertical dashed line). The diagnostics used to constrain the OSM interpretive model are identified in Figure 1. Target Langmuir probe (LP) arrays and edge Thomson scattering [10] provide radial n_e and T_e profiles in the divertors and upstream, respectively. The non-steady core density corresponds to a particle growth rate of $8.3 \times 10^{20} \text{ D}^+ \text{ s}^{-1}$ (from the \bar{n}_e slope in Figure 2 and a plasma volume of

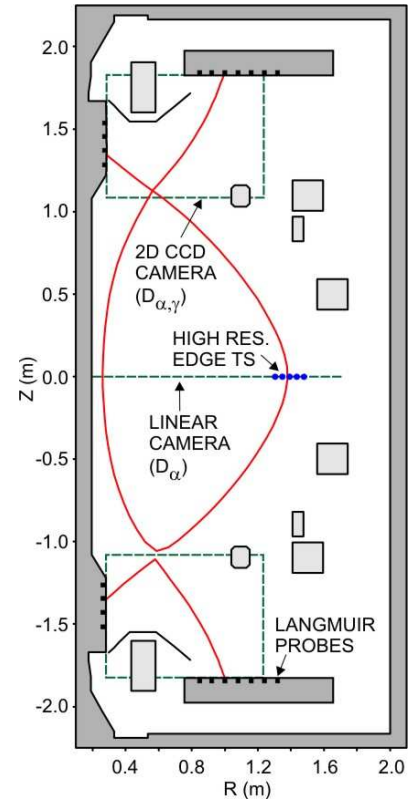


Figure 1: MAST poloidal cross section and relevant diagnostics. The separatrix location for 17469 at 259 ms is also shown.

8.0 m^{-3}), but this is only $\sim 10\%$ of the total recycling flux of $9.7 \times 10^{21} \text{ D}^+ \text{ s}^{-1}$ (from the LP data) and is therefore not explicitly included in the particle balance analysis. D_α constraints are provided by 1D (linear) CCD midplane and 2D CCD divertor camera systems, with the data inverted to provide profiles in the poloidal plane.

Results

The model agrees with the D_α measurements to within experimental uncertainties, which are $\sim 30\%$, suggesting that neutral transport in the divertors and main chamber are represented in the simulation with “reasonable accuracy”. Figure 3 plots the volume averaged ionisation source in the confined plasma as a function of poloidal distance around the LCFS, with the origin at the upper x-point and proceeding clockwise. The locations of the outer midplane (dotted line) and lower x-point (dashed line) are marked. Aside from the absence of fuelling at the inner midplane, the x-point dominated structure in the poloidal distribution is perhaps unexpected given the open divertor and remote wall design of MAST, where the neutral density outside the plasma is generally assumed to be uniform. The volume averaged radial profiles are shown in Figure 4 (solid lines). Outer midplane radial profiles (dashed) are also plotted to illustrate the factor ~ 2 error in pedestal transport analysis for this discharge if it was based on midplane data alone, which can be the case for 1D core models given the difficulty in resolving poloidal dependencies.

The outer midplane fast ionisation gauge provides an independent check of the simulation since the main neutral sources (recycling and beams) and sinks (plasma and surface pumping) in the region of the gauge are fully specified by the experimental data set input to the model. The measured molecular density is $2.2 \times 10^{18} \text{ D}_2 \text{ m}^{-3}$, with an estimated uncertainty of 30–50%, and the model result of $8.1 \times 10^{17} \text{ D}_2 \text{ m}^{-3}$ is lower by 63%. This discrepancy may simply result from gauge calibration but might also indicate an underestimate of the neutral source, perhaps from a modest error in the recycling flux measurement, a wall source associated with H-mode operation, or thermal D_2 leakage from the neutral beam injector. The inclusion of these “missing” neutrals, at a level sufficient to resolve the gauge discrepancy, still allows agreement within the error bounds of the D_α data.

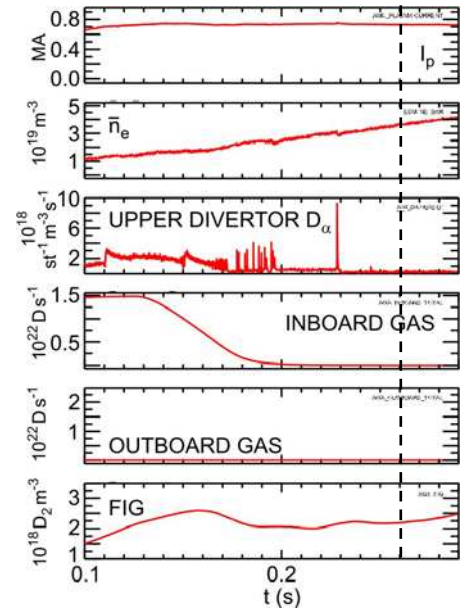


Figure 2: Time-traces for 17469. “FIG” refers to fast ionisation gauge. The simulation is for the plasma state at 259 ms.

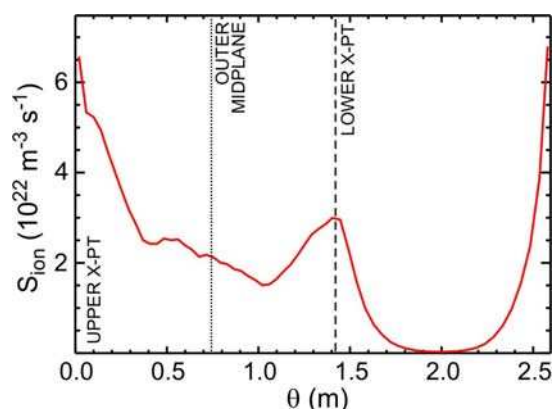


Figure 3: Calculated poloidal distribution of ionisation in the confined plasma (volume averaged) for 17469. The OSM-Eirene model is highly constrained by experimental data.

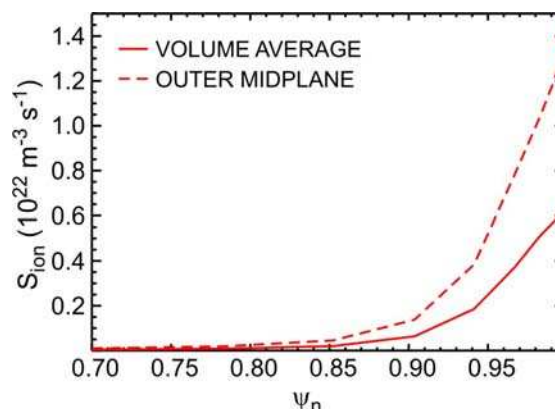


Figure 4: Radial distributions of ionisation in the confined plasma, with the volume averaged profile (solid) compared to the outer midplane profile (dashed).

Future work

The next step in the analysis will involve estimation of the pedestal cross-field transport coefficients for particles, improvement of the data set (in particular the incorporation of 2D main-chamber D_α measurements), and the study of inter-ELM density pedestal evolution.

Acknowledgements

This work was funded jointly by the United Kingdom Engineering and Physical Sciences Research Council and by the European Communities under the contract of Association between EURATOM and UKAEA. Contributions were also made by the Natural Sciences and Engineering Research Council of Canada via the Special Research Opportunity program.

References

- [1] A. Loarte *et al.*, Nucl. Fusion 47, S241 (2007)
- [2] P. C. Stangeby, J. Appl. Phys. 36, 2784-2788 (2003)
- [3] R. J. Groebner *et al.*, Fus. Sci. Technol. 48 (2), (2005)
- [4] M. A. Mahdavi, R. Maingi *et al.*, Phys. Plasmas 10, 3984 (2003)
- [5] L.D. Horton, A.V. Chankin1 *et al.*, Nucl. Fusion 45, 856–862 (2005)
- [6] S. Lisgo *et al.* J. Nucl. Mater. 337, 139-145 (2005)
- [7] D. Reiter, <http://www.eirene.de>
- [8] G. F. Counsell *et al.*, Nucl. Fusion 45, S157 (2005)
- [9] A.W. Morris, R.J. Akers *et al.*, Fusion Eng. Design 74, 67-75 (2005)
- [10] R. Scannell, M. J. Walsh *et al.*, Rev. Sci. Instrum. 77, 10E510 (2006)